Role of Metal Nanoparticles in TiO 2 /Ag Nanocomposite-Based Microheterogeneous Photocatalysis

ARTICLE *in* THE JOURNAL OF PHYSICAL CHEMISTRY B · JULY 2004

Impact Factor: 3.3 · DOI: 10.1021/jp0379751

6 AUTHORS, INCLUDING:

Davide Cozzoli
Università del Salento
136 PUBLICATIONS **5,721** CITATIONS
SEE PROFILE

Roberto Comparelli
Italian National Research Council
120 PUBLICATIONS **1,417** CITATIONS
SEE PROFILE

M. L. Curri
Italian National Research Council
245 PUBLICATIONS **3,354** CITATIONS
SEE PROFILE

Angela Agostiano
Università degli Studi di Bari Aldo Moro
358 PUBLICATIONS **4,074** CITATIONS
SEE PROFILE

Role of Metal Nanoparticles in TiO_2/Ag Nanocomposite-Based Microheterogeneous Photocatalysis

P. Davide Cozzoli,[†] Elisabetta Fanizza,[†] Roberto Comparelli,[†] M. Lucia Curri,[‡] and Angela Agostiano*[,†,‡]

Dipartimento di Chimica, Università di Bari, Via Orabona 4, 70126 Bari, Italy, and CNR-Istituto per i Processi Chimico Fisici (IPCF), sez. Bari, Via Orabona 4, 70126 Bari, Italy

Danièle Laub[§]

EPFL-CIME-Centre Interdisciplinaire de Microscopie Electronique, Batiment MXC, 1015 Lausanne, Switzerland

Received: December 22, 2003; In Final Form: March 9, 2004

The photocatalytic performance of anatase TiO_2 nanorod-stabilized Ag nanoparticles has been investigated during the reductive bleaching of a model dye, Uniblue A (UBA), in homogeneous organic solutions. The activity of the TiO_2/Ag nanocomposite has been found to vary continuously during the course of photocatalysis, following a concomitant light-induced modification of the metal nanoparticle size and size distribution. The direct involvement of the metal particles in mediating electron transfer between photoexcited TiO_2 and the target UBA is explained on the basis of the size-dependent redox properties of the metal nanoparticles. The present results can be useful in the design of new composite materials with well-tailored photocatalytic properties and long-term stability.

1. Introduction

Major efforts in modern material chemistry are devoted to the design and fabrication of nanostructured systems with tunable physical−chemical properties for advanced catalytic applications. Recent discoveries on the improved technological performances obtainable by coupling different nanostructured materials have encouraged research toward exploring the potential offered by noble metal/semiconductor oxide nanocomposites in catalysis.[1−7]

In the nanosized regime, as the oxide function can strongly deviate from its conventional role as simple support, unusual or enhanced catalytic activity[2] can be indeed detected due to specific metal−oxide electronic interactions.[3−5] Furthermore, the interest in combining noble metal nanoparticles with semiconductor oxides basically relies on the metal ability in acting both as a sink for electrons and as redox catalyst. Noble metal nanoparticles have been recognized to promote electron-transfer processes,[8−10] as demonstrated in seed-mediated metal growth mechanisms[10b,11] and metal-catalyzed reduction of organic compounds.[9a,b,10a] Photoinduced charge carrier separation[5−7] can be actually favored in semiconductor/metal nanocomposites, as proved by the enhancement of photocatalytic[5,6] and photoelectrochemical[7] performances in such combined materials.

In the field of photocatalysis, most recent studies have focused on the characterization of the nanocomposites before irradiation or just following short laser pulse excitation.[6a−c] Little or no information is available on whether the initial properties of semiconductor/metal composites are retained upon long-term light exposure.[5b,c,6b,c,7c] For example, because of their high photoactivity, noble metal nanoclusters can be expected to undergo size−shape transformation when subjected to intense light.[12,13] Moreover, metal cluster etching, based on oxygen-driven chemical[11a,b,15] and photochemical dissolution,[6b,15] is known to be facile, especially in the presence of strong ligands for the metal ions[11b] and/or of electron scavengers.[6b,12d,e] Recognition of such processes is of paramount importance, as they may originate a nanostructured material whose catalytic activity can vary during the course of photocatalysis. Accordingly, the size-regime dependence of catalytic reactions has been largely emphasized in the literature.[3a,b,9a,b,10,14] Further investigations are undoubtedly needed in order to rationalize the performances of such composite materials, as it has been also found that during photocatalysis, a semiconductor/metal nanojunction may not necessarily facilitate electron discharge into the solution.[6b,d,e,7a]

In the present work, the morphological changes occurring to a TiO_2/Ag nanocomposite material have been followed during steady-state photocatalysis in order to establish a relationship between the overall photocatalytic activity of the nanocomposite and the metal particle size upon long-term UV illumination. Recently synthesized TiO_2 nanorod-stabilized Ag nanoparticles[15] have been employed as a convenient semiconductor/metal photocatalyst to easily follow the elementary steps involved in organics reductive photodegradation. Such nanocomposite appears suitable to this purpose for several reasons. First, the TiO_2 nanorod−Ag nanoparticle composite is soluble in organic media, providing a macroscopically homogeneous (i.e., without phase boundaries) photocatalyst dispersion, which however remains heterogeneous at the nanoscale. More importantly, the resulting solution is optically transparent, thus allowing the course of

* To whom correspondence should be addressed. Fax: +39-080-5442129/5442209. E-mail: csildc28@area.ba.cnr.it; agostiano@area.ba.cnr.it.
[†] Università di Bari.
[‡] CNR-Istituto per i Processi Chimico Fisici (IPCF).
[§] EPFL-CIME-Centre Interdisciplinaire de Microscopie Electronique.

10.1021/jp0379751 CCC: $27.50
Published on Web 06/05/2004

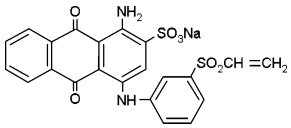

Figure 1. Molecular structure of Uniblue A.

photocatalytic reactions to be monitored spectrophotometrically. The optical monitoring of the electrons accumulation process in the nanocomposite during photoexcitation of the semiconductor may be also experimentally accessible, thus providing a complementary tool to evaluate the redox activity of the system as a function of irradiation time. Second, the metal nanoparticles possess "clean" surfaces,[15] i.e., not coordinated by surfactant molecules. As an advantage, undesired loss of catalytic activity can be prevented, as blocking of surface active sites[16] and ligand sterical hindrance to the access of reactants to the metal are limited. Finally, as opposed to the case of small metal islands that are typically deposited onto semiconductor nanocrystals,[6a−f] the eventual structural evolution of segregated metal nanoparticles can be easily followed by TEM.[6g,h,15]

For the purposes of our study, the performances of TiO_2/Ag photocatalysts with metal particles of different initial size are compared with that of the bare TiO_2 nanorods during the reductive bleaching of a model dye, Uniblue A (UBA), under UV illumination. UBA[17] is chosen as a model substrate for probing electron-transfer reactions mediated by metal nanoparticles as its decoloration by TiO_2 conduction band electrons is favored thermodynamically,[10,18] also being accompanied by specific absorption changes.[18b] It is found that as the Ag mean particle size and size distribution vary during the course of photocatalysis, the dye bleaching rate becomes affected to a different extent, thus reflecting the direct involvement of the metal particles in the overall catalytic process. The role of the Ag nanoparticles in mediating electron transfer between photoexcited TiO_2 and the target UBA is explained on the basis of the size-dependent redox properties of the metal nanoparticles.

2. Experimental Section

2.1. Chemicals. All chemicals were of the highest purity available and used as received without further purification. Silver nitrate ($AgNO_3$, 99.998%), Uniblue A (UBA, sodium salt, M_w 506.49, see Figure 1), titanium tetraisopropoxide ($Ti(OPr^i)_4$ or TTIP, 99.999%), trimethylamino-*N*-oxide dihydrate ($(CH_3)_3NO\cdot 2H_2O$ or TMAO, 98%), trimethylamine ($(CH_3)_3N$ or TMA, water solution), tetramethylammonium hydroxide ($(CH_3)_4NOH$ or TMAH, water solution), tetrabutylammonium hydroxyde ($(C_4H_9)_4NOH$ or TBAH, water solution), and oleic acid ($C_{18}H_{33}CO_2H$ or OLEA, 90%) were purchased from Aldrich. All solvents used were of analytical grade and purchased from Aldrich.

2.2. Preparation of Photocatalyst. *Synthesis of Anatase TiO_2 Nanorods.* Organic-capped anatase TiO_2 nanorods were synthesized by hydrolysis of titanium tetraisopropoxide (TTIP) using oleic acid (OLEA) as surfactant, as previously reported.[19] Briefly, an excess of aqueous base (TMAO, TMA, TMAH, or TBAH) solution was injected in a single portion into a OLEA/TTIP solution at 80−100 °C. Rodlike TiO_2 nanocrystals were grown in 6−12 h, after which they could be readily precipitated upon addition of an excess of ethanol to the growing mixture at room temperature. The precipitate was isolated by centrifugation and washed three times with ethanol to remove surfactant residuals. The resulting OLEA-capped TiO_2 nanocrystals were homogeneously dispersed in chloroform solutions, due to their high solubility in nonpolar organic media.

Synthesis of TiO_2/Ag Nanocomposites. Optically clear solutions of TiO_2/Ag nanocomposites were prepared by employing TiO_2 nanorods as stabilizers for silver nanoparticles in nonpolar media without addition of specific organic ligands for the metal. Segregated Ag nanoparticles were produced upon photocatalytic reduction of $AgNO_3$, according to a previously reported procedure.[15] Briefly, a quartz cuvette was filled with a solution containing the desired concentration of TiO_2 (expressed with reference to the TTIP precursor concentration) and $AgNO_3$ in $CHCl_3$:EtOH mixtures (EtOH content was 2−10% v/v). $AgNO_3$ concentration ranged between 10^{-6} and 10^{-3} M, while TiO_2 concentration was between 10^{-1} and 10^{-4} M. The colloidal stability of the nanocomposites was ensured by keeping the TiO_2:$AgNO_3$ molar ratio in the range 100:1−5:1. The cuvette was sealed by a Teflon-faced rubber cap and subsequently deaerated by gently purging the solution with nitrogen for 30 min. Then, the cuvette was UV-irradiated under stirring by using a 200 W mercury lamp ($\lambda > 300$ nm). The Ag nanoparticle size and size distribution could be modulated by simply adjusting the irradiation time. A detailed optical and morphological characterization of the as-prepared TiO_2 nanorod-stabilized Ag nanoparticles can be found in ref 15.

2.3. Photocatalyzed Decolorization of Uniblue A in Homogeneous Solution. In a typical experiment, the starting reaction mixture (in $CHCl_3$:EtOH 90:10 v/v) was prepared in a glovebox by adding a deaerated Uniblue A ethanolic solution to the desired volume of a freshly prepared photocatalyst solution (either TiO_2, TiO_2/$AgNO_3$, or a preformed TiO_2/Ag nanocomposite solution). The establishment of an adsorption−desorption equilibrium for the dye was assumed to be fast. Oxygen-free conditions were employed in order to both preserve the organic-capping layer on the titania surface against photooxidation and prevent the silver nanoparticles from photodissolution.[15] A quartz cuvette was thus filled with the reaction mixture and sealed by a Teflon-faced rubber cap in the glovebox. The mixture was kept under stirring and UV-irradiated using a high-pressure 200 W mercury lamp ($\lambda > 300$ nm). The light intensity was adjusted by placing neutral density filters on the light path to avoid direct dye photolysis. The system was arranged in a suitable geometry in order to monitor the reaction course in situ. The illumination was stopped during absorption measurements. Aliquots of the solution were withdrawn via a syringe at scheduled time intervals and immediately used for imaging the photocatalyst by TEM.

For a comparison, analogous UBA bleaching experiments were also performed by using the visible light of a 200 W quartz tungsten−halogen lamp ($\lambda < 340$ nm was cut by a suitable glass filter): in these cases, UBA bleaching was never detected on the same time scale as that of the corresponding UV-photocatalytic experiments.

2.4. Characterization Techniques. *UV−vis Absorption Spectroscopy.* UV−vis absorption spectra were recorded with an Ocean Optics UV−vis diode array spectrophotometer equipped with an optical fiber, a deuterium lamp, and a tungsten−halogen lamp.

Electrochemistry. Cyclic voltammetry of UBA probe dye was performed by an AUTOLAB PGSTAT10 potentiostat interfaced with a personal computer. The reference electrode was Ag/AgCl ($E^0 = 0.222$ V vs NHE); the counter and working electrodes were a platinum wire and glassy carbon, respectively. Tetrabutylammonium perchlorate was used as supporting electrolyte. A typical scan rate was 500 mV/s.

Transmission Electron Microscopy. Transmission electron microscopy (TEM) images were obtained using a Philips EM

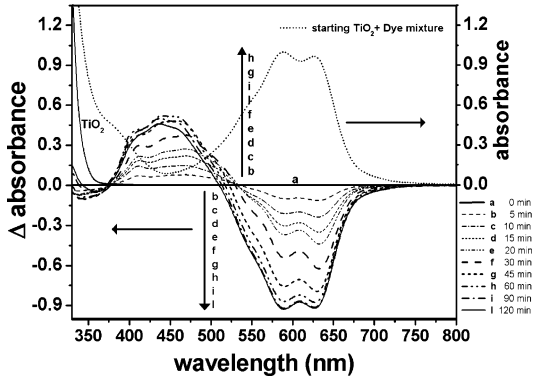

Figure 2. Time-dependent evolution of the absorption spectrum (left axis) of an UBA/TiO_2 nanorods solution ([UBA] = 10^{-5} M, [TiO_2] = 5×10^{-3} M) in a N_2-saturated $CHCl_3$:EtOH (90:10 v/v) mixture upon UV irradiation. The baseline (line a) was adjusted to zero absorbance using the unphotolyzed TiO_2 + dye mixture. The absorption spectrum of the sole TiO_2 nanoparticles and that of initial mixture are also shown (right axis).

430 microscope (TEM) operating at 300 kV. The samples for the analysis were prepared by dropping dilute solutions of freshly synthesized TiO_2/Ag nanocomposite onto 400-mesh carbon-coated copper grids and leaving the solvent to dry. The samples were stable under the electron beam and did not degrade within the typical observation times.

3. Results

3.1. Redox Properties of UBA. The redox properties of UBA were first studied by cyclic voltammetry in $CHCl_3$:EtOH = 90:10 v/v solution. In the negative potential range, UBA gave two irreversible redox couples. The corresponding half-wave potentials $E^0_{1/2}$ were measured at −0.372 and −0.591 V (vs NHE), respectively. The reduction peaks were attributed[20] to the sequential reduction of the carbonyl groups of antraquinonic moiety of UBA (see Figure 1) to sequentially yield the semi-antraquinonic and hydroantraquinonic derivatives.

3.2. Photocatalyzed Reduction of UBA by TiO_2 Conduction Band Electrons. UBA is a convenient substrate to probe TiO_2-initiated photoreduction reactions as it exhibits a different color in its reduced form,[18b] basically arising from the different electron conjugation in the antraquinonic and hydroantraquinonic moiety.

The feasibility of UBA reduction by the TiO_2 photogenerated conduction band electrons in organic media was demonstrated by the following experiment (see Supporting Information) according to a previously reported method.[18a] A deaerated ethanolic 1 M TiO_2 nanorod suspension was first irradiated. The solution turned from milk-white to blue at the naked eye in a few minutes (Figure 1S, Supporting Information). Such coloration is known to result from the trapping of the photogenerated electrons within the semiconductor nanocrystallites.[18a,21] The excess electrons remained as long as an inert atmosphere was maintained in the quartz vessel, as oxygen could quickly scavenge the accumulated electrons. In a glovebox, a fixed amount of this titania suspension (1 mL) was added to deaerated ethanolic UBA solutions (3 mL) with varying dye concentration (Figure 2S-a, Supporting Information). Immediately after mixing in the dark, a color change of the overall mixture occurred. After centrifugation of the suspension, (Figure 2S-b, Supporting Information), the supernatant exhibited a yellow color, while careful inspection of the TiO_2 precipitate revealed the presence of both white and blue powder in each reaction batch. In contrast, unirradiated TiO_2 did not induce any dye discoloration. Immediately after aerating the solutions, the remaining TiO_2 blue powder recovered its original white color (Figure 2S-c, Supporting Information). In general, upon continuous UBA addition, increasing dye amounts could be decolored as long as some blue titania was present. Beyond this point, due to the full consumption of the stored electrons, further UBA addition resulted in excess dye in the solution.

As a confirmation, upon direct UV irradiation of deaerated EtOH suspensions of TiO_2/UBA, similar spectral changes accompanied the dye bleaching (data not shown) while the TiO_2 powder was observed to turn blue only after the dye decoloration was complete.

Finally, upon exposure of the bleached solution to air in the dark, the initial UBA absorption features were fully recovered in 24−72 h, depending on the starting dye concentration.

For the purposes of the present study, TiO_2-photocatalyzed UBA reduction was carried out in homogeneous $CHCl_3$/EtOH solutions. By employing TiO_2 nanorods from the same preparation batch, three different sets of experiments were compared in which the active photocatalysts were (i) *TiO_2 nanorods*; (ii) *TiO_2 nanorods/$AgNO_3$*, in this case, the silver particles were generated in situ during UV illumination; (iii) *preformed TiO_2/Ag nanocomposites*, the nanocomposite solution was prepared in a separate photocatalytic synthesis and then added to the dye. In all cases, the concentration of titania and silver, expressed with reference to the parent species, TTIP and $AgNO_3$, respectively, was kept constant.

However, a complication arises from the structured absorption of the dye byproducts that is mainly located in the 350−500 nm region where the silver plasmon (SP) strongly absorbs. In principle, one way to compensate for such SP interferences would be the use of an irradiated blank solution (i.e., containing only the photocatalyst) as the reference. As preliminary experiments showed that the silver SP intensity, position, and width were significantly affected by adsorption of both the dye and its byproducts in a manner difficult to predict, this method could not correctly discriminate UBA (or its byproducts) absorption from that of the metal nanoparticles. Therefore, in our investigation, difference absorption spectra of the irradiated reaction mixtures were recorded by using the respective unphotolyzed solution as the reference. The comparison between the TiO_2- and TiO_2/Ag-catalyzed UBA bleaching is reported and discussed as representative of the relative trend of the photodegradation course rather than of its exact quantitative estimation.

(i) TiO_2 Nanorod-Catalyzed Photoreduction. The experiments were carried out in N_2-saturated $CHCl_3$ solutions containing 10−15% v/v ethanol. These conditions ensured titania colloidal stability for at least 7−9 h, i.e., the nanorods retained their perfect solubility for a period much longer than the typical time course of UBA bleaching process. Hole scavenging by ethanol, in fact, preserves the organic-capping on the TiO_2 nanocrystal surface from its inevitable UV-photocatalyzed degradation, ultimately resulting in the precipitation of the nanocrystal from the solution.[15] In contrast to the corresponding ethanolic suspensions, TiO_2 in $CHCl_3$/EtOH mixed solvent did not exhibit any noticeable absorption changes upon prolonged UV irradiation.

In Figure 2 the course of Uniblue A photodegradation catalyzed by TiO_2 nanorods in deaerated $CHCl_3$:EtOH mixture is reported. The spectrum of the starting TiO_2/Dye mixture (short dotted line, right axis, solvent as the reference) exhibited two characteristic peaks at λ'_{max} = 588 nm and λ''_{max} = 625 nm, while the spectral features below 400 nm remained masked by the intense absorption of TiO_2. The TiO_2 nanorods catalyzed a

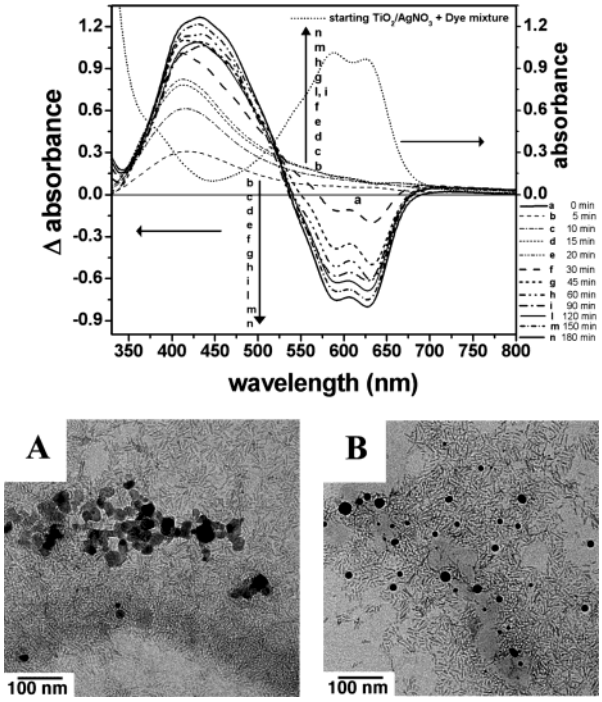

Figure 3. (Top) Time-dependent evolution of the absorption spectrum of an UBA/$AgNO_3$/TiO_2 nanorods solution ([UBA] = 10^{-5} M, [TiO_2] = 5×10^{-3} M, [$AgNO_3$] = 5×10^{-5} M) in N_2-saturated $CHCl_3$:EtOH (90:10 v/v) mixture upon UV irradiation. The baseline (line a) was adjusted to zero absorbance using the unphotolyzed $TiO_2/AgNO_3$ + dye mixture. The absorption spectrum of the initial mixture is also shown (right axis). (Bottom) TEM overview of the TiO_2/Ag nanocomposites at t =10 (A) and 30 min (B).

progressive absorption bleaching in the 500−700 nm visible region (line b−l, left axis) over about 90 min. This bleaching corresponds to the disappearance of ground-state dye as it is converted into its reduced form. Simultaneously, a prominent structured absorption grew up in the 390−510 nm region, attributable to the dye byproducts. These absorption features were rather broadened when compared to those detected in EtOH (Figure 3S, Supporting Information). This fact was mainly attributed to the different polarity of the medium, as demonstrated by the fact that the absorption of UBA byproducts obtained in EtOH changed after diluting 90:10 v/v with deaerated $CHCl_3$, ultimately resembling the absorption of UBA byproducts obtained in $CHCl_3$:EtOH mixtures.

In aerated solutions, UBA photobleaching exhibited identical behavior, but it occurred at a slower rate (150 min).

Further experiments were carried out by varying the EtOH content in the mixtures and/or adding an •OH radical scavenger (2-propanol, 1−4 M). No significant difference in the evolution of UBA absorption spectrum as well as in the overall degradation rate was observed. Nevertheless, a quantitative spectrophotometric determination of the dye concentration by comparison with standard solutions could not be accurately made. The dye byproducts, in fact, interfere with a low absorption tail at $\lambda > 500$ nm, as it can be seen in the spectra when the pure solvent is used as the reference.[18b] As a result, in the difference spectra, a slightly lower UBA bleaching than the actual one was measured in the visible region, owing to the positive byproducts absorption contribution. Accordingly, the relative ratio between the bleaching values at λ'_{max} and λ''_{max} varied during photocatalysis.

(ii) TiO_2 Nanorods/$AgNO_3$-Catalyzed Photoreduction. In Figure 3 (top) the course of UBA photodegradation catalyzed by TiO_2 nanorods in deaerated $CHCl_3$ containing $AgNO_3$ is reported. Since the beginning, an asymmetric broad band was seen centered at around 430 nm, which slightly blue-shifted while increasing in magnitude (lines b−e). As in the initial mixture there was no reduced metal silver, such a relatively large band could be attributed to the surface plasmon (SP)[8,26] of the in-situ-generated Ag nanoparticles. Notably, the SP appeared remarkably broadened when compared to Ag photocatalytic synthesis in the absence of UBA,[15] likely because of dye adsorption onto the metal surface. The dye decoloration was seen to start only after a 20 min induction period, being recognized by an absorption bleaching superimposed on the plasmon tail (lines e−n) at 500−700 nm. At the same time, in the 410−550 region, the SP band was no more clearly distinguishable due to the superimposition of the dye byproducts absorption.

As a general trend, the overall reaction rate was slower when compared to the Ag-free photodegradation as it took about 180 min to reach the maximum dye bleaching. This behavior was found to be remarkably accentuated with increasing the initial $AgNO_3$ concentration.

The morphological transformation of the formed silver clusters was investigated by extracting aliquots from the reaction mixture at different illumination times and imaging them by TEM. Figure 3 (bottom) reports representative TEM images of the TiO_2 nanorods/Ag nanocomposite at t = 10 (A) and 30 min (B). As it can be seen, the silver clusters are generally found associated with areas of the carbon grid that are overcrowded with titania nanocrystals. Because of the significantly lower image contrast characterizing TiO_2 when compared to Ag, the silver nanoparticles can be easily identified as dark spots superimposed on an underlying titania background.[15] As opposed to the titania nanoparticles, the Ag particles appeared in different dimensional and/or morphological regimes during the course of illumination. At the early stages of $AgNO_3$ photoreduction (A), relatively large and highly agglomerated Ag clusters were detected, comprising irregularly shaped particles of about 50−15 nm. In the later stages of UBA photodegradation (B), well-separated and widely polydispersed Ag particles (20 ± 10 nm) could be observed, among which a high fraction (>50%) of small particles (15−18 nm) was present.

(iii) Preformed TiO_2/Ag Nanocomposite-Catalyzed Photoreduction. A set of UBA degradation experiments was performed by irradiating a solution containing preformed TiO_2 nanorods/Ag nanocomposite as photocatalyst. TiO_2/Ag nanocomposite were employed in which the metal particles had different mean sizes and size distributions.

A representative photoreduction experiment is reported in Figure 4 (top). The initial absorbance value of UBA visible band (short dotted line, right axis, spectrum vs solvent) was slightly higher than that in Figure 2, obviously because of the additional contribution of the SP band. Notably, although there was no induction period for UBA degradation to start, the disappearance of the dye double band was significantly slower in the earliest (lines b−f) than in the latest irradiation period (lines g−l). In addition, the time necessary to reach the maximum UBA bleaching in the 500−700 nm region remained comparable to that found in the photoreduction without Ag (cfr. lines i−l in Figure 5). During the course of the photoreaction, a strong absorption could be seen to grow in the 390−510 nm range, attributable to both UBA byproducts and the relative change in silver SP absorption due to the progressive metal nanoparticle photofragmentation.[15] This latter fact was confirmed by TEM investigations. Figure 4 (bottom) shows typical TEM pictures of the nanocomposite catalyst at different UBA bleaching times.

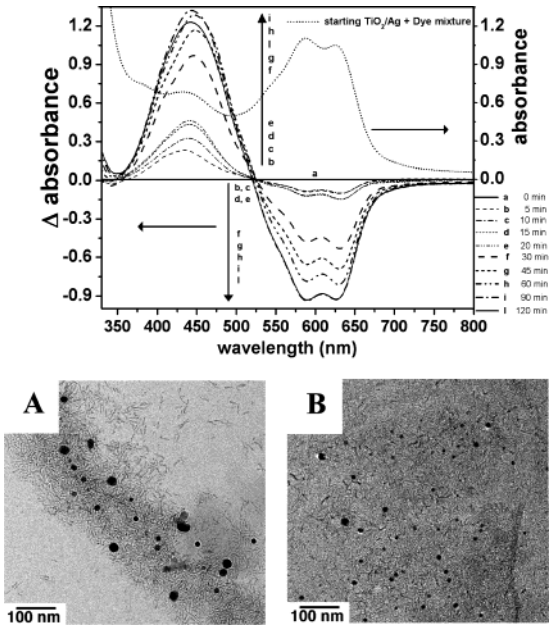

Figure 4. (Top) Time-dependent evolution of the absorption spectrum of an UBA/Ag/TiO_2 nanorods solution ([UBA] = 10^{-5} M, [TiO_2] = 5 × 10^{-3} M, [Ag] =5 × 10^{-5} M) in N_2-saturated $CHCl_3$:EtOH (90:10 v/v) mixture upon UV irradiation. The baseline was adjusted to zero absorbance (line a) using the unirradiated TiO_2/Ag + dye mixture. The absorption spectrum of the initial mixture is also shown (right axis). (Bottom) TEM overview of the TiO_2/Ag nanocomposites at $t = 0$ (A) and 30 min (B).

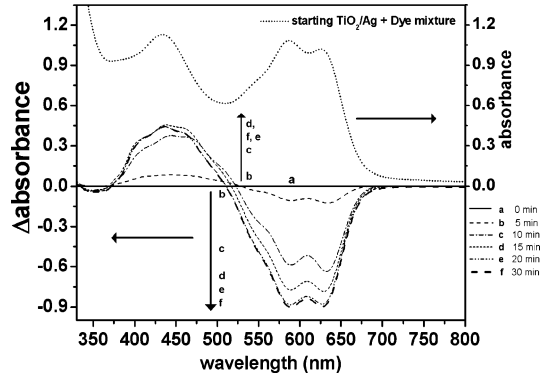

Figure 5. Time-dependent evolution of the absorption spectrum of an UBA/Ag/TiO_2 nanorods solution ([UBA] = 10^{-5} M, [TiO_2] = 5 × 10^{-3} M, [Ag] = 5 × 10^{-5} M) in a N_2-saturated $CHCl_3$:EtOH (90:10 v/v) mixture upon UV irradiation. A TEM overview of the starting TiO_2/Ag catalyst used for this experiment is shown in Figure 4B. The baseline (line a) was adjusted to zero absorbance using the unphotolyzed TiO_2/Ag/dye mixture. The absorption spectrum of the initial mixture is also shown (right axis).

As it can be seen, the initial photocatalyst (A) contained Ag nanoparticles with a relatively large mean particles size and a rather broad size distribution (25 ± 10 nm). In the later stages of UBA bleaching (B), definitely smaller and more uniformly sized particles (10 ± 2 nm) were present in the mixture.

As a general trend, for a given photocatalyst sample with an initial broad size distribution of Ag nanoparticles, the higher the silver concentration at constant TiO_2 content, the longer the initial time period during which the photoreduction rate was slowed. After that, a considerable enhancement of the degradation rate was usually detected.

In contrast, when 10 ± 2 nm silver particles were present in the initial reaction mixture, the overall UBA photoreduction (Figure 5) was extremely fast (about 20 min). Notably, in the 390−510 nm region, the absorption changes reflected exclusively the formation of the dye byproducts, as for the experiment in Figure 5. This result agreed with previously reported data[15] which highlighted that 8−10 nm Ag particles remained stable in size for long irradiation periods, thus showing no significant SP absorption changes. This explains why the SP contribution could not be detected in the difference spectra. In this case, the reaction rate could be increased by increasing the silver concentration up to 10-fold, above which the degradation rate decreased.

Finally, at the end of the all above-described photocatalytic experiments in homogeneous phase, it was observed that the original UBA absorption features were slowly (24−72 h) restored if air was admitted into the quartz cuvette kept in the dark. When metal Ag was present in the solution, the nanoparticles simultaneously underwent a progressive oxidative dissolution under oxygen atmosphere, in agreement with previously reported results.[15]

4. Discussion

Band-gap excitation of TiO_2 generates valence band holes and conduction band electrons (eq 1). Under normal conditions, the redox potential of the photogenerated e_{CB}^- is not negative enough (e_{CB}^-, $E^0 = -0.5$ V vs NHE at pH 7) for efficient reduction reactions[22,23]

$$TiO_2 + h\nu \rightarrow TiO_2\,(e_{CB}^- + h_{VB}^+) \quad (1)$$

As a result, most of studies on aqueous TiO_2 photocatalysis have focused on hydroxyl radical-initiated oxidations, whereas CB electron direct reductive pathways have been largely neglected.[24,25] In contrast, a deaerated $CHCl_3$/EtOH mixture represents an ideal medium where reduction reactions can be strongly enhanced, owing to an efficient hole scavenging by the solvent (eqs 2 and 3), to suppression of •OH radical production and to the reducing action of CB electrons and CH_3-CH•OH radicals[15,18,21]

$$C_2H_5OH + h_{VB}^+ \text{ (or } \bullet OH) \rightarrow CH_3CH\bullet OH + H^+ \text{ (or } H_2O) \quad (2)$$

$$CHCl_3 + h_{VB}^+ \text{ (or } \bullet OH) \rightarrow \bullet CCl_3 + H^+ \text{ (or } H_2O) \quad (3)$$

In the following discussion, we approximate the standard redox potential E^0 for some half reactions to the corresponding half-wave potential value $E_{1/2}$ present in the literature data as it has been often practiced by other authors.[24] We also assume that the literature redox potential scale, measured for aqueous media, is reasonably valid for our system.[20b]

The measured UBA redox potential indicates that its direct reduction by CB electrons or by $CH_3CH\bullet OH$ radicals (E^0 for the $CH_3CHO/CH_3CH\bullet OH$ couple is −0.94 V vs NHE[25e]) is thermodynamically allowed. Actually, although UBA oxidation by VB holes (h_{VB}^+, $E^0 = +2.7$ V vs NHE at pH 7) is also possible (E^0 for UBA_{ox}/UBA is 1.038 V[17b] vs NHE), such a process can be largely inhibited under our photobleaching conditions by the efficient hole transfer to ethanol, the latter being present in large excess with respect to UBA.

The surfactant-coated TiO_2 nanorods did not exhibit any absorption changes upon UV illumination when dissolved in deaerated $CHCl_3$ or $CHCl_3$/EtOH mixture, whereas titania ethanolic suspensions turned blue due to accumulation of the photogenerated electrons within the titania nanocrystals. In the latter case, electron storage in the semiconductor results from the selective hole scavenging by the solvent and/or from electron

injection by $CH_3CH•OH$ radicals.[18a,21] In contrast, direct $CHCl_3$ oxidation by holes may not be likewise efficient, while in $CHCl_3$/EtOH mixture consumption of photogenerated CB electrons can occur even under N_2 through direct reduction of $•CCl_3$ radicals ($E^0 \approx 0$ V) to $:CCl_2$ by e_{CB}^- or by $CH_3CH•OH$ radicals, ultimately leading to CO (upon reaction with H_2O traces in the solvent) and dimerization products.[25] Such a redox-mediated short-circuiting of the photogenerated charge carriers could reasonably contribute in further preventing CB electrons from accumulating onto the semiconductor. Accordingly, it has been previously reported that e_{CB}^- cannot be stored in the TiO_2 particles as long as electron acceptor molecules are present in the bulk solution.[18a]

The primary involvement of TiO_2 conduction band electrons in the UBA-photocatalyzed bleaching was demonstrated by the following observations. First, UBA decoloration occurred in the dark by reaction with blue titania colloids, being characterized by the same spectral changes as those detected during steady-state UV illumination. This can actually be accounted for only by scavenging of the trapped electrons by the dye, the latter being, in turn, reduced. Accordingly, once all stored electrons were consumed, no further increase in the dye reduction could be observed. Second, the presence of other efficient electron scavengers, such as dissolved O_2 or Ag^+, greatly slowed the UBA bleaching, while the addition of •OH scavengers had no effect on the decoloration rate. Third, the initial dye absorption could be restored upon slow reoxidation of its byproducts by ambient O_2, regardless of the nature of the solvent employed in the photocatalytic experiments. As is well-known in the pertaining literature,[20] the occurrence of this oxygen-driven back-reaction reasonably indicates that the UBA bleaching process should basically involve the reduction carbonyl groups of antraquinonic moiety of UBA to yield the corresponding hydroanthraquinoic product. Although the addition of $:CCl_2$ or $•CCl_3$ to the terminal $SO_2CH{=}CH_2$ double bond of UBA might also occur during photocatalysis, the related products are not expected to modify significantly the dramatic absorption changes ascribable to the formation of the sole hydroanhraquinonic UBA derivative.

All the above-reported evidence suggests that CB electrons participate in the bleaching process. As a confirmation, it has been reported[18b] that when experimental conditions (e.g., in aerated aqueous titania) favor UBA oxidative photodegradation, absorption changes in UBA spectrum (λ'_{max} and λ''_{max} blue shifted to 455 and 490 nm, respectively) are consistent with the formation of UBA hydroxylated derivatives. The temporal evolution of UBA spectrum is, in fact, completely different in our experiments. Finally, the ethanol content in the $CHCl_3$:EtOH mixtures did not affect the bleaching rate significantly, thus indicating that secondary reduction by $CH_3CH•OH$ radicals is only a minor pathway in the UBA decoloration.

Our experiments undoubtedly demonstrated that the presence of silver nanoparticles in the TiO_2/Ag photocatalyst affected the photoreduction rate to a considerable extent.

When the initial TiO_2/UBA reaction mixture contained $AgNO_3$, the dye bleaching started once electrons were no longer utilized for Ag^+ reduction

$$Ag^+ + e_{CB}^- \rightarrow Ag^0 \qquad (4)$$

$$Ag^+ + CH_3CH•OH \rightarrow Ag^0 + CH_3CHO + H^+ \qquad (5)$$

The higher the initial $AgNO_3$ concentration, the longer the induction period. This proved that CB electrons uptake by Ag^+ and by the dye did not occur simultaneously. At the beginning of UBA decoloration, large particles were found in solution. The dye bleaching proceeded rather slowly until the population of smaller particles increased in the solution.

SCHEME 1: Scheme of Energy Levels in Photoirradiated TiO_2 Quantum Dot−Metal Nanojunction

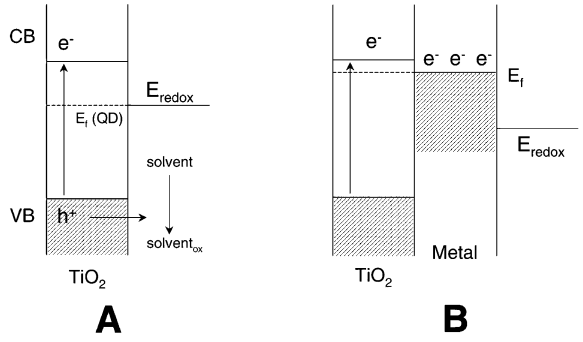

Analogous qualitative behavior was found when preformed TiO_2/Ag nanocomposites were present in the starting mixture. The dye decoloration started immediately in these cases as there were no unreacted Ag^+ ions. However, the reaction rate appeared remarkably slowed down in the early stages when compared with the degradation catalyzed by unmodified TiO_2. The delay in the dye bleaching was fully recovered in the subsequent stages when a larger fraction of smaller Ag particles was present in solution in comparison with the starting reaction mixture. Accordingly, the smaller the mean silver particle size in the initial photocatalyst, the faster the maximum UBA bleaching was reached. When the starting catalyst contained the smallest (8−10 nm) particles attainable by the employed photocatalytic method,[15] the UBA degradation rate exceeded the decay rate observed with the sole TiO_2 nanorods.

A mechanism for the photocatalytic reduction of UBA can be proposed by considering the known processes occurring at a semiconductor−metal nanojunction. They are summarized in Scheme 1. The Fermi level E_F in an open-circuit semiconductor nanoparticle is poorly defined but will be in the midgap region (A), and in principle, its position is dictated by the most facile redox couple present in solution (dotted line). Before illumination, a TiO_2 nanoparticle will contain no electrons in the conduction band. UV irradiation produces electron/hole pairs. If the holes are rapidly scavenged by the solvent, excess electron can accumulate in the oxide (blue color of the TiO_2 colloid) and the Fermi level moves toward the CB edge. A TiO_2/Ag nanojunction is not ohmic in nature:[6e] once all Ag^+ ions are reduced, photogenerated electrons can flow from the semiconductor to the metal where they, in fact, accumulate due to the slow transfer to the solvent. Additional electrons can be further injected by reducing $CH_3CH•OH$ radicals. As demonstrated earlier,[5−7] in such nanojunctions, electrons are stored overwhelmingly on the metal because the Helmholtz capacitance of the metal solution is much higher than the space charge capacity of the semiconductor nanocrystal, even under accumulation. As a consequence, the Fermi level in silver is shifted cathodically until it can eventually equilibrate with the TiO_2 Fermi level (B). The phenomenon of electron accumulation in metal can be recognized by detectable SP absorption changes (red shift and band intensity decrease).[8e,15] In the presence of better electron acceptors than the solvent molecules, the metal nanoparticles can readily release the accumulated electrons.

The observed behavior during UBA photoreduction can be reasonably related to the "dynamic" morphology of the photocatalytic system. As a matter of fact, the UBA degradation rate

SCHEME 2: Scheme of the Mechanism for Ag-Mediated Electron Transfer from Photoexcited TiO_2 to the Dye[a]

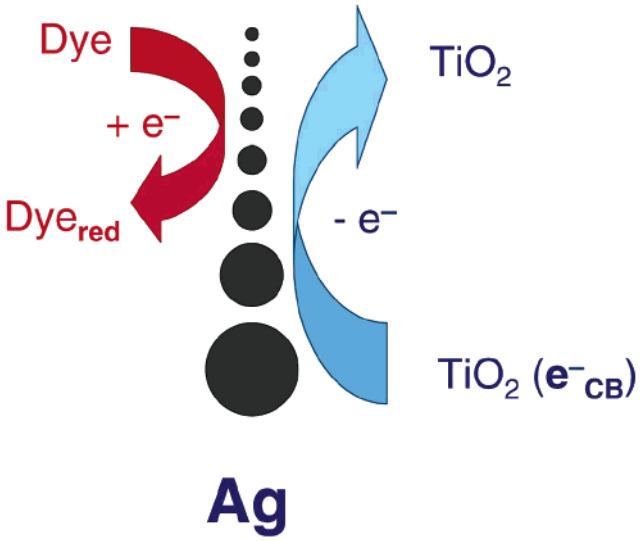

[a] Photoexcited electrons readily transfer from TiO_2 to the metal nanoparticles, but their subsequent release to the dye occurs only via the smaller metal nanoparticles.

varies continuously during illumination following light-induced modifications[12,13] of the mean Ag particle size and size distribution.[15] The existence of an induction period before the reaction rate stabilizes at its full value points to a minimum particle size requirement for an efficient catalysis.

The characteristic slowing of the UBA degradation rate in the presence of silver particles can be explained by a simple redox mechanism involving an initial competition between UBA and the Ag nanoparticles for the reducing sources (Scheme 2). Although electron accumulation on the metal particles is facile, the subsequent electron may not be likewise favored. An efficient redox catalysis, in fact, requires that the potential of the metal particles must be more negative than that of the acceptor dye. The higher this difference, the larger the driving force for electron transfer. It can be reasonably suggested that for a given Ag nanoparticle population, only the fraction of clusters smaller than a critical dimension possesses a redox potential that is negative enough to reduce UBA. The higher catalytic activity of smaller particles when compared to larger ones arises from the combination of their inherently lower redox potential with their enhanced capability of storing electrons because of the higher surface-to-volume ratio. This explains why the degradation rate is greatly enhanced as the number of smaller clusters increases. Further, only in experiments where most particles have the minimum attainable size (~8−10 nm), the dye degradation rate is much faster at any stage than the corresponding reaction catalyzed by unmodified titania.

In earlier investigations of metal nanoparticle-mediated redox catalysis, it has been emphasized that a high electron injection capability of the reducing agent is essential to shift the metal particle redox potential to highly negative values. Interestingly, although the nucleophilicity of the electron sources in our photocatalytic system is limited as compared with other efficient nucleophiles (for example, $E_0 = -1.3$ V for $NaBH_4$), it is sufficient to sustain the Ag potential at less negative values than the potential of UBA, even with larger silver particle sizes than previously reported.[9a,b] The absence of organic-capping ligand at the silver particles surface and a continuously renewable metal surface can be also invoked as additional factors accounting for the higher catalytic activity of smaller clusters.

Nevertheless, the observation that the higher the Ag particles concentration at constant TiO_2 content, the longer the initial time period during which the photoreduction rate was slowed, seems to contradict the concept of a minimum size requirement. An increase in the total silver concentration should, in fact, imply a higher concentration of smaller particles, i.e., of the most catalytically active nanoparticles. This result may be explained by considering an initial transfer of titania CB electrons mainly to the larger Ag particles possessing a lower Fermi lever but less catalytic activity, while prolonged light absorption at $\lambda > 350$ nm by the latter is required to induce their progressive conversion into smaller ones.[12a,b,13a] Accordingly, these effects are much less pronounced for the light-stable small Ag nanoparticles.

5. Conclusions

An attractive technique for the reductive decoloration of dyes has been presented that can be potentially extendable to the photocatalytic treatment of a variety organic compounds. The present study has revealed that the photocatalytic activity of the TiO_2/Ag nanocomposite under steady-state irradiation can vary continuously during the course of photocatalysis due to a concomitant light-induced modification of the initial metal nanoparticle size and size distribution. This fact can be taken into account in the design of new photocatalysts with well-tailored efficiency and long-term stability.

Acknowledgment. The authors thank Dr. Pinalysa Cosma for assistance in electrochemical measurements.

Supporting Information Available: Figures depicting de-aerated ethanolic TiO_2 nanorod suspensions before and after UV illumination, ethanolic UBA solutions with increasing dye concentration, and absorption spectra of the ethanolic UBA solutions. This material is available free of charge via the Internet at http://pubs.acs.org.

References and Notes

(1) (a) Rolison, D. R. *Science* **2003**, *299*, 1698. (b) Bell, A. T. *Science* **2003**, *299*, 1688. (c) Schmid, G. *Clusters and Colloids: From Theory to Application*; VCH: Weinheim, 1994. (d) Kamat, P. V. *Prog. React. Kinet.* **1994**, *19*, 277. (e) Zhang, J. Z. *Acc. Chem. Res.* **1997**, *30*, 423. (f) Kamat, P. V. Composite Semiconductor Nanoclusters. In *Semiconductor Nanoclusters- Physical, Chemical and Catalytic aspects;* Kamat, P. V., Meisel, D., Eds.; Elsevier Science: Amsterdam, 1997; p 237.

(2) (a) Rao, C. N. R.; Vijayakrishnan, V.; Santra, A. K.; Prins, M. W. J. *Angew. Chem., Int. Ed. Engl.* **1992**, *31*, 1062. (b) Valden, M.; Lai, X.; Goodman, D. W. *Science* **1998**, *281*, 1647. (c) Xu, C.; Lai, X.; Zajac, G. W.; Goodman, D. W. *Phys. Rev. B* **1997**, *56*, 13464.

(3) (a) Roucoux, A.; Schlz, J.; Patin, H. *Chem. Rev.* **2002**, *102*, 3757. (b) Lewis, L. N. *Chem. Rev.* **1993**, *93*, 2693. (c) Kiwi, J.; Gratzel, M. *J. Am. Chem. Soc.* **1979**, *101*, 7214. (d) Brugger, P. A.; Cuendet, P.; Gratzel, M. *J. Am. Chem. Soc.* **1981**, *103*, 2923. (e) Reets, M. T.; Helbig, W. *J. Am. Chem. Soc.* **1994**, *116*, 7401. (f) Wang, Q.; Liu, H.; Wang, H. J. *Colloid Interface Sci.* **1997**, *190*, 380. (g) Szucs, A.; Berger, F.; Dekany, I. *J. Colloid Interface Sci.* **2000**, *174*, 387. (h) Claus, P.; Hofmeister, H. *J. Phys. Chem. B* **1999**, *103*, 2766.

(4) (a) Ma, Q.; Klier, K.; Cheng, H.; Mitchell, J. W.; Hayes, K. S. *J. Phys. Chem. B* **2001**, *105*, 9230. (b) Xu, B.-Q.; Wei, J.-M.; Yu, Y.-T.; Li, Y.; Li, J.-L.; Zhu, Q.-M. *J. Phys. Chem. B* **2003**, *107*, 5203. (c) Dong, W.; Feng, S.; Shi, Z.; Li, L.; Xu, Y. *Chem. Mater.* **2003**, *15*, 1941. (d) Soejima, T.; Tada, H.; Kawahara, T.; Ito, S. *Langmuir* **2002**, *18*, 4191.

(5) (a) Gerischer, H. *J. Phys. Chem.* **1984**, *88*, 6096. (b) Sun, B.; Vorontsov, A. V.; Smirniotis, P. G.; Smirniotis, G. *Langmuir* **2003**, *19*, 3151. (c) Einaga, H.; Harada, M.; Futamura, S.; Ibusuki, T. *J. Phys. Chem.* **2003**, *107*, 9290.

(6) (a) Dawson, A.; Kamat, P. V. *J. Phys. Chem. B* **2001**, *105*, 960. (b) Subramanian, V.; Wolf, E.; Kamat, P. V. *Langmuir* **2003**, *19*, 469. (c) Kamat, P. V.; Flumiani, M.; Dawson, A. *Colloids Surf. A* **2002**, *202*, 269.

(d) Wood, A.; Giersig, M.; Mulvaney, P. *J. Phys. Chem. B* **2001**, *105*, 8810. (e) Subramanian, V.; Wolf, E. E.; Kamat, P. V. *J. Phys. Chem. B* **2003**, *107*, 7479. (f) Sun, B.; Vorontsov, A. V.; Smirniotis, P. G.; Smirniotis, G. *Langmuir* **2003**, *19*, 3151. (g) Zhang, L.; Yu, C. Y.; Yip, H. Y.; Li, Q.; Kwong, K. W.; Xu, A.-W.; Wong, P. K. *Langmuir* **2003**, *19*, 10372. (h) Zhang, F.; Guan, N.; Li, Y.; Zhang, X.; Chen, J.; Zeng, H. *Langmuir* **2003**, *19*, 8230.

(7) (a) Jakob, M.; Levanon, H.; Kamat, P. V. *Nano Lett.* **2003**, *3*, 353. (b) Chandrasekharan, N.; Kamat, P. V. *J. Phys. Chem. B* **2000**, *104*, 10851. (c) Stathatos, E.; Lianos, P.; Falaras, P.; Siokou, A. *Langmuir* **2000**, *16*, 2398. (d) Subramanian, V.; Wolf, E.; Kamat, P. V. *J. Phys. Chem. B* **2001**, *105*, 11439. (e) Haick, H.; Paz, Y. *J. Phys. Chem. B* **2003**, *107*, 2319. (f) Chandrasekharan, N.; Kamat, P. V.; Hu, J.; Jones, G., II *J. Phys. Chem. B* **2000**, *104*, 11103.

(8) (a) Link, S.; El-Sayed, M. A. *J. Phys. Chem. B* **1999**, *103*, 8410. (b) El-Sayed, M. A. *Acc. Chem. Res.* **2001**, *34*, 257. (c) Kamat, P. V. *J. Phys. Chem. B* **2002**, *106*, 7729. (d) Toshima, N. *Pure Appl. Chem.* **2000**, *72*, 317.

(9) (a) Jana, N. R.; Sau, T. K.; Pal, T. *J. Phys. Chem. B* **1999**, *103*, 115. (b) Pradhan, N.; Pal, A.; Pal, T. *Langmuir* **2001**, *17*, 1800. (c) Ghosh, S. K.; Kundu, S.; Mandal, M.; Pal, T. *Langmuir* **2002**, *18*, 8756. (d) Claus, P.; Hofmeister, H. *J. Phys. Chem. B* **1999**, *103*, 2766. (e) Sudrik, S. G.; Maddanimath, T.; Chaki, N. K.; Chavan, S. P.; Chavan, S. P.; Sonawane, H. R.; Vijayamohanan, K. *Org. Lett.* **2003**, *5*, 2355.

(10) (a) Jana, N. R.; Pal, T. *Langmuir* **1999**, *15*, 3458. (b) Sau, T. K.; Pal, A.; Pal, T. *J. Phys. Chem. B* **2001**, *105*, 9266. (c) Li, Y.; Boone, E.; El-Sayed, M. A. *Langmuir* **2002**, *18*, 4921.

(11) (a) Henglein, A. *Chem. Mater.* **1998**, *10*, 444. (b) Henglein, A. *Langmuir* **2001**, *17*, 2329.

(12) (a) Kamat, P. V.; Flumiani, M.; Hartland, G. V. *J. Phys. Chem. B* **1998**, *102*, 3123. (b) Ah, C. S.; Han, H. S.; Kim, K.; Jang, D.-J. *J. Phys. Chem. B* **2000**, *104*, 8153. (c) Ah, C. S.; Han, H. S.; Kim, K.; Jang, D.-J. *Pure Appl. Chem.* **2000**, *72*, 91. (d) Linnert, T.; Mulvaney, P.; Henglein, A. *Ber. Bunsen-Ges Phys. Chem.* **1991**, *95*, 838. (e) Murakoshi, K.; Tanaka, H.; Sawai, Y.; Nakato, Y. *J. Phys. Chem. B* **2002**, *106*, 3041.

(13) (a) Jin, R. C.; Cao, Y. W.; Mirkin, C. A.; Kelly, K. L.; Schatz, G. C.; Zheng, J. G. *Science* **2001**, *294*, 1901. (b) Jin, R.; Cao, Y. C.; Hao, E.; Metraux, G.; Schatz, G. C.; Mirkin, C. A. *Nature* **2003**, *425*, 487.

(14) (a) Li, Y.; El-Sayed, M. A. *J. Phys. Chem. B* **2001**, *105*, 8938. (b) Narayanan, R.; El-Sayed, M. A. *J. Am. Chem. Soc.* **2003**, *125*, 8340. (c) Jana, N. R.; Wang, Z. L.; Pal, T. *Langmuir* **2000**, *16*, 2457.

(15) Cozzoli, P. D.; Comparelli, R.; Fanizza, E.; Curri, M. L.; Agostiano, A.; Laub, D. *J. Am. Chem. Soc.* **2004**, *126*, 3868.

(16) (a) Kapoor, S. *Langmuir* **1999**, *15*, 4365. (b) Li, Y.; El-Sayed, M. A. *J. Phys. Chem. B* **2001**, *105*, 8938. (c) Narayanan, R.; El-Sayed, M. A. *J. Am. Chem. Soc.* **2003**, *125*, 8340. (d) Jana, N. R.; Wang, Z. L.; Pal, T.; *Langmuir* **2000**, *16*, 2457. (e) Schmid, G.; West, H.; Mehles, H.; Lehnert, A. *Inorg. Chem.* **1997**, *36*, 891. (f) Yeung, L. K.; Croooks, R. M. *Nano Lett.* **2001**, *1*, 14.

(17) (a) McCallum, J. E. B.; Madison, S. A.; Alkan, S.; Depinto, R. L.; Wahl, R. U. R. *Environ. Sci. Technol.* **2000**, *34*, 5157. (b) Herrera, F.; Kiwi, J.; Lopez, A.; Nadtochenko, V. *Environ. Sci. Technol.* **1999**, *33*, 3145.

(18) (a) Vinodgopal, K.; Bedja, I.; Hotchandani, S.; Kamat, P. V. *Langmuir* **1994**, *10*, 1767. (b) Cozzoli, P. D.; Comparelli, R.; Fanizza, E.; Curri, M. L.; Agostiano, A. *Mater. Sci. Eng. C* **2003**, *23*, 707.

(19) Cozzoli, P. D.; Kornowski, A.; Weller, H. *J. Am. Chem. Soc.* **2003**, *125*, 14539.

(20) (a) Dryhurst, G.; Kadish, K. M.; Scheller, F.; Renneberg, R. *Biological Electrochemistry*; Academic Press Inc.: New York, 1982, Vol 1, pp 1−115. (b) *International Critical Tables of Numerical Data, Physics, Chemistry and Technology*; McGraw-Hill Book Co., Inc.: New York and London, 1929; Vol. VI, pp 333−335.

(21) Kamat, P. V.; Bedja, I.; Hotchandani, S. *J. Phys. Chem.* **1994**, *98*, 9137. (b) Safrany, A.; Gao, R.; Rabani, J. *J. Phys. Chem. B* **2000**, *104*, 5848.

(22) (a) *Advanced Catalysis and Nanostructured Materials*; Moser, W. R., Ed.; Academic Press: San Diego, 1990. (b) *Photocatalysis and Environment, Trends and Applications*; Schiavello, M., Ed.; Kluwer: Dordrecht, 1988. (c) *Photocatalysis. Fundamentals and Applications*; Pelizzetti, E., Serpone, N., Eds.; Wiley: New York, 1989.

(23) (a) Colon, G.; Hidalgo, M. C.; Navio, J. A. *Langmuir* **2001**, *17*, 7174. (b) Colon, G.; Hidalgo, M. C.; Navio, J. A. *J. Photochem. Photobiol.* **2001**, *138*, 79. (c) Sato, S.; Ueda, K.; Kawasaki, Y.; Nakamura, R. *J. Phys. Chem. B* **2002**, *106*, 9054. (d) Tada, H.; Teranishi, K.; Ito, S. *Langmuir* **1999**, *15*, 7084. (e) Hoffman, M. R.; Martin, S. T.; Choi, W.; Bahnemann, D. F. *Chem. Rev.* **1995**, *95*, 69. (f) Mills, A.; Le Hunte, S. *J. Photochem. Photobiol. A* **1997**, *108*, 1.

(24) (a) Schmelling, D. C.; Gray, K. A.; Kamat, P. V. *Environ. Sci. Technol.* **1996**, *30*, 2547. (b) Calhoun, K. L.; Winkelmann, K.; Millis, G. *J. Phys. Chem. B* **2001**, *105*, 9739. (c) Bae, E.; Choi, E. *Environ. Sci. Technol.* **2003**, *37*, 147.

(25) (a) Choi, W.; Hoffmann, M. R. *Environ. Sci. Technol.* **1997**, *31*, 89. (b) Kormann, C.; Bahnemann, D. W.; Hoffmann, M. R. *Environ. Sci. Technol.* **1991**, *25*, 494. (c) Choi, W.; Hoffmann, M. R. *J. Phys. Chem.* **1996**, *100*, 12161. (d) Stark, J.; Rabani, J. *J. Phys. Chem. B* **1999**, *103*, 8524. (e) Choi, W.; Hoffmann, M. R. *Environ. Sci. Technol.* **1995**, *29*, 1646.

(26) (a) Mulvaney, P. *Langmuir* **1996**, *12*, 788. (b) Dickson, R. M.; Lyon, L. A. *J. Phys. Chem. B* **2000**, *104*, 6095. (c) Sun, Y.; Xia, Y. *Science* **2002**, *298*, 2176. (d) Jin, R. C.; Cao, Y. W.; Mirkin, C. A.; Kelly, K. L.; Schatz, G. C.; Zheng, J. G. *Science* **2001**, *294*, 1901. (f) Callegari, A.; Tonti, D.; Chergui, M. *Nano Lett.* **2003**, *3*, 1565. (g) Maillard, M.; Huang, P.; Brus, L. *Nano Lett.* **2003**, *3*, 1611. (h) Zhang, H.; Zelmon, D. E.; Deng, L.; Liu, H.-K.; Teo, B. K. *J. Am. Chem. Soc.* **2001**, *123*, 11300. (i) Wang, W.; Asher, S. A. *J. Am. Chem. Soc.* **2001**, *123*, 12528. (l) Sun, Y.-P.; Riggs, J. E.; Rollins, H. W.; Guduru, R. *J. Phys. Chem. B* **1999**, *103*, 77. (m) Zheng, J.; Dickson, R. M. *J. Am. Chem. Soc.* **2002**, *124*, 13982.